Alkali Reduction of Graphene Oxide in Molten Halide Salts: Production of Corrugated Graphene Derivatives for High-Performance Supercapacitors

Amr M. Abdelkader,* Cristina Vallés, Adam J. Cooper, Ian A. Kinloch, and Robert A. W. Dryfe

University of Manchester, Manchester M13 9PL, United Kingdom

ABSTRACT Herein we present a green and facile approach to the successful reduction of graphene oxide (GO) materials using molten halide flux at 370 °C. GO materials have been synthesized using a modified Hummers method and subsequently reduced for periods of up to 8 h. Reduced GO (rGO) flakes have been characterized using X-ray-diffraction (XRD), Raman spectroscopy, X-ray photoelectron spectroscopy (XPS), thermogravimetric analysis (TGA) and Fourier transform infrared spectroscopy (FTIR), all indicating a significantly reduced amount of oxygen-containing functionalities on the rGO materials. Furthermore, impressive electrical conductivities and electrochemical capacitances have been measured for the rGO flakes, which, along with the morphology determined from scanning electron microscopy, highlight the role of surface corrugation in these rGO materials.

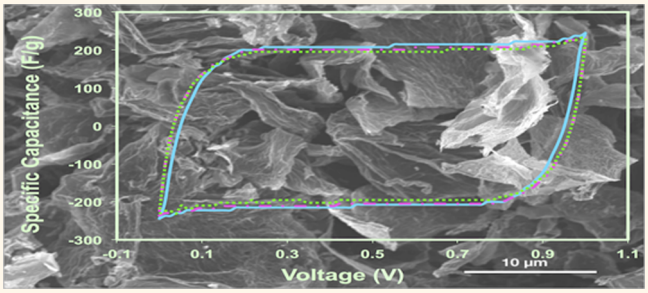

KEYWORDS: graphene oxide · molten halide · metallothermic reduction · surface corrugation

Graphene, a two-dimensional lattice with monatomic thickness constructed of a hexagonal array of sp^2 carbon atoms, has recently gained significant interest in major areas of scientific research since its first isolation in 2004 by Geim and Novoselov *via* the "scotch tape" method.[1] Graphene's unique structure allows for optimized electrical and mechanical properties, such as high electrical conductivity and a high charge carrier mobility (20 $m^2/V/s$) due to the extensive electron delocalization caused by the complete sp^2 nature of the carbon lattice. Because graphene is a two-dimensional material, it has a maximum specific surface area of 2630 $m^2\ g^{-1}$,[1] excellent tensile strength (130 000 N mm^{-2}),[2] impressive elasticity, superior thermal conductivity (5000 W $m^{-1}\ K^{-1}$)[3] and a Young's modulus close to 1 TPa.[3] Furthermore, since graphene is primarily carbon based, it has a broad electrochemical potential window and is >97% optically transparent.[4,5]

These excellent properties have enabled graphene to qualify as a potential candidate as an electrode material in future electrical and electrochemical applications, including next generation electronics,[6] sensors,[7] energy storage materials,[8] electrocatalysts, composites,[9] and ultrastrong paper-like materials. However, future industrial applications heavily rely on the development of scalable, high purity processing methods. Present routes reported for graphene synthesis span a range of methods, including the prolonged sonication of graphite powder in nonaqueous media,[10] sonication of graphite intercalation compounds, cathodic exfoliation of graphite through intercalation/deintercalation processes,[11−13] and oxidative exfoliation of a graphite anode.[14] However, although reported work is often entitled "graphene production", the products of these methods are often few-layer and/or oxidized materials, limiting their use in future applications. At present, there is currently no method of producing high yield, single-layer pristine graphene flakes of a practical lateral size.

Graphene oxide (GO) has been suggested as a precursor for large-scale production of

* Address correspondence to amr.abdelkader@manchester.ac.uk.

Received for review July 2, 2014 and accepted October 22, 2014.

Published online October 22, 2014
10.1021/nn505700x

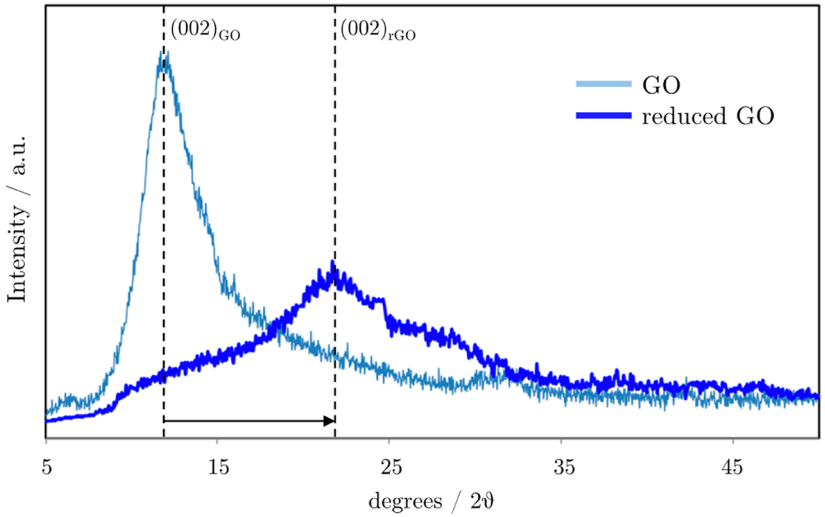

Figure 1. Single crystal XRD diffraction patterns for as prepared GO and reduced GO performed, *via* alkali metal reduction, highlighting the (002) diffraction peaks of both GO and rGO as well as the shift caused by the reduction process.

monolayer graphene. Graphene oxide is essentially an oxidized graphene sheet, densely, but randomly, decorated with hydroxyl and epoxy groups. Through removal of these oxygen-containing functional groups by chemical reduction, a conductive sheet of graphene is obtained. However, it is generally accepted that reversibility of the high electrical conductivity lost during initial oxidation of the graphene sheets is challenging, and the reduced GO typically has a lower electrical conductivity than its parent material. Nonetheless, GO reduction has only partially been investigated, and it would be premature to completely dismiss due to the numerous possible approaches available toward the reduction of GO.

Several reduction methods for GO have been reported. Thermal reduction is a relatively simple and "green" approach.[15,16] However, the high temperature and the long reduction periods make the process energy intensive.[15] Moreover, structural damage was reported on the graphene sheets due to the release of gaseous carbon dioxide.[15] It has been found that reducing GO with hydrogen gas improves the quality of the resulting graphene, but elevated temperatures are required (>1000 °C).

Wet chemical reduction, using reducing agents such as hydrazine,[17] sodium borohydride,[18] hydrogen sulfide,[19] HI,[20,21] dimethylhydrazine,[9] and hydroquinone,[22] can take place at room temperature, but some of these reagents are extremely hazardous and may introduce additional functionalization during the reduction process.[17,23] Furthermore, the majority of chemical reduction processes are complicated and time-consuming (up to 24 h).[17,18] The reduction of GO using metal powder dissolved in HCl solutions offers a more environmentally friendly reduction procedure.[24−26] However, it is difficult to avoid the contamination of graphene with metal ions, and the graphene sheets agglomerate into clusters composed of 2−10 stacked individual monatomic graphene layers.[24−26] Therefore, a simple, low cost, eco-friendly process remains in demand, and is essential for obtaining high-quality reduced graphene oxide for scalable production.

Herein we report an efficient, green and facile approach to reduce GO using alkali metals in molten halide flux at 400 °C. In addition to being eco-friendly, our process has several credible advantages over the alternative aforementioned chemical routes, such as the associated high yield, low cost, and short time processing. The present paper takes the lithiothermic reduction of GO in molten KCl-LiCl as proof of concept. However, the reduction with alternative alkali metals is readily performed and will be discussed in future work.

RESULTS AND DISCUSSION

The XRD patterns of the original GO and reduced GO are shown in Figure 1. Because of the presence of hydroxyl, epoxy and carboxyl groups bound to the graphene sheets, the interplanar spacing of GO, calculated from the observed position of the (002) peak (2θ = 10.3°), corresponds to a *d*-spacing of *ca*. 0.8 nm (*cf*. 0.34 nm for graphite). After removal of the oxygenated functional groups from the graphene sheets *via* alkali metal reduction, the (002) peak is seen to shift to greater 2θ values coinciding with a decrease in the peak intensity, indicating that a significant degree of conjugation within the graphene network (sp^2 carbon) is restored during the reduction process. This is associated with the ring-opening of the epoxides.

Raman spectroscopy is a powerful analytical tool for probing the electronic structure of chemical compounds and is widely used to characterize the crystal structure, disorder and lattice defects in carbon-based nanomaterials. Particularly within graphene research, it

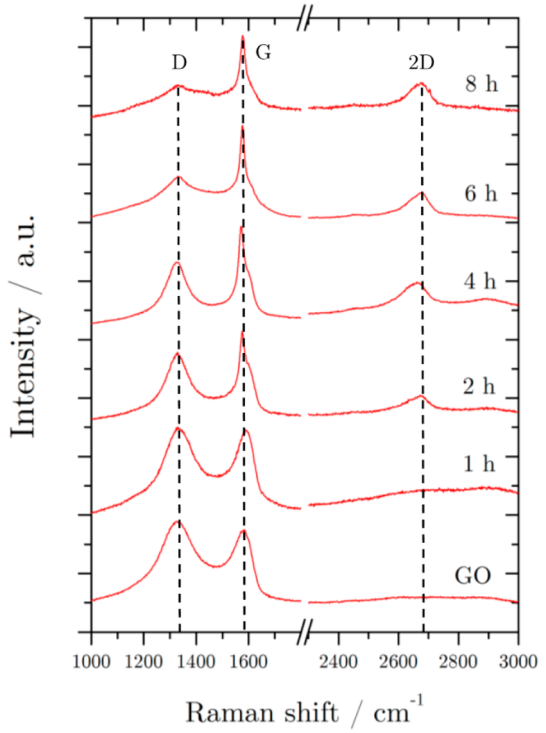

Figure 2. Raman spectroscopy of GO and reduced GO showing how the Raman spectra change, highlighting the three main Raman signals: *D*, *G*, and *2D* bands, with increasing reaction times. The *2D* band can be clearly seen to become more prominent as the reduction reaction proceeds.

is the initial point of call for determining the number of graphene layers. It can be seen from Figure 2 that the Raman spectrum of GO is characterized by the associated broadening of two familiar bands observed in Raman spectroscopy of graphene: the *G* band at *ca.* 1585 cm^{-1} and the *D* mode peak centered on *ca.* 1330 cm^{-1}. The *G* peak results from the first order scattering of the E_{2g} phonon of sp^2 carbon hybridization and is therefore prominent in all graphite-based materials. The *G* band merges with another band, the *D*′ band (centered on *ca.* 1600 cm^{-1}) at high defect concentrations, which are caused by surface oxidation. The *D* peak, arising from the breathing mode of K-point phonons of A_{1g} symmetry in graphene, is broad and intense due to the reduction in size of the in-plane sp^2 domain caused by extensive oxidation. Post reduction, the intensity of the *D* band decreases as a function of the reduction time due to the recovery of the sp^2 network. After 8 h reduction, the I_D/I_G of the reduced GO is *ca.* 0.22. This value is significantly lower than that reported in the literature. Significantly, another band at *ca.* 2660 cm^{-1} begins to appear after 4 h of reduction, and its intensity was found to increase proportionally with the reduction time. This band, known as *2D* or *G*′ band, arises from the second order of zone-boundary phonons and is activated by a two-phonon (opposite momentum) assisted double resonance process. Thus, pristine graphene with a perfect sp^2 hybridization

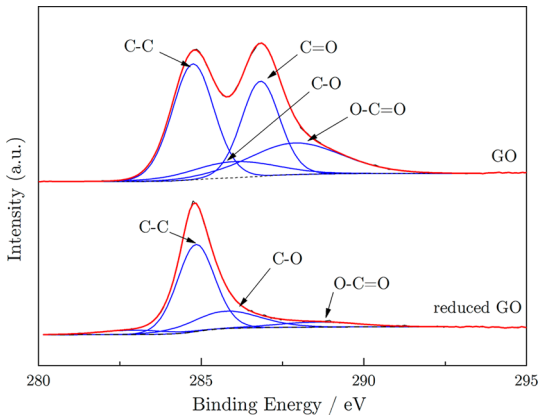

Figure 3. XPS spectra of as-prepared GO (top) and reduced GO (bottom) showing a significant reduction in the amount of oxygen containing functional groups on the graphene sheets from the reduction process.

network and no lattice defects displays a very strong *2D* signal, for which the intensity is inversely proportional to the defect concentration. Hence, the *2D* band is not observed for GO materials or, to our knowledge, for the reduced forms of GO prepared by any other reported method due to the remaining functional groups and defects.[27] The presence of this peak, albeit for only *ca.* 40% of the recorded spectra, is evidence to support the removal of oxygen containing functional groups in the graphene lattice without inducing defects into the reduced GO structure.

X-ray photoelectron spectroscopy (XPS) was employed to probe the degree of chemical functionalization and to quantify the subsequent GO reduction. The effectiveness of the reduction process can be described using the measured carbon to oxygen ratio of the reduction products, which is obtained from the C 1s to O 1s peak areas from the XPS data. In brief, the C 1s XPS spectrum of GO (Figure 3) clearly indicates a considerable degree of oxidation fitted to four components, corresponding to carbon atoms bound in several different states: in-plane sp^2 carbon, C−O bound carbon, carbonyl carbon, and carboxylate carbon (O−C−O). The C 1s XPS spectrum of GO is consistent with previous reports,[28] and the peak at *ca.* 284.5 eV arises from sp^2 and sp^3 carbon stretching modes. Finally the higher binding energy components, of which intensities are greatly decreased on reduction, arise from the carbon−oxygen binding energies.

The C/O atomic ratio calculated from the XPS results is increased from C/O = 2.2 for GO up to C/O = 7 for the treated material. The degree of oxidative functionality is clearly reduced in the treated material compared to that in the GO.

The thermal stability of the GO and rGO was investigated through the use of thermogravimetric analysis (TGA). TGA plots of GO and RGO are shown in Figure 4 and the GO curve exhibits two major weight losses at *ca.* 175 and 450 °C. The lower temperature weight loss

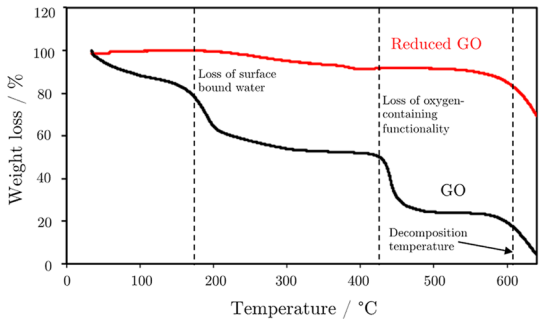

Figure 4. TGA curves obtained for both GO and reduced GO showing an enhanced thermal stability for reduced GO, indicated by the significantly smaller weight losses attributed to water and oxygen-containing functionality, at the respective temperatures.

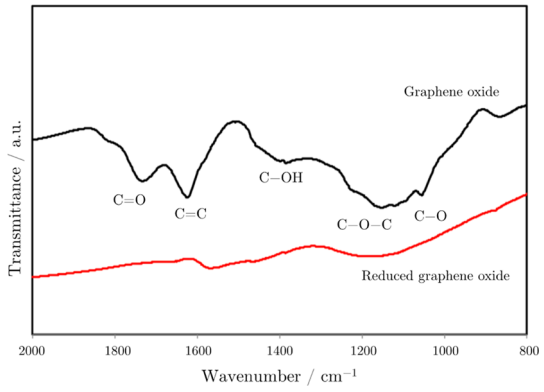

Figure 5. FTIR spectra for GO and reduced GO showing significantly decreased intensities in the labeled oxygen-related FTIR features, on reduction of GO.

is due to water molecules adsorbed at the GO bulk material, whereas the higher temperature weight loss can be attributed to the elimination of most of the oxygen-containing functional groups.[28] Further weight loss occurs up to the decomposition temperature and can be associated with the removal of more stable oxygen functionalities. The total weight loss up to the decomposition temperature was calculated to be *ca.* 77%. Reduced GO on the other hand, exhibits an enhanced thermal stability and the total weight loss before the full decomposition was only *ca.* 10%. This slight weight loss could be attributed to the presence of surface-adsorbed water, but it is clear that the lower degree of functionality is reflected by the fewer decomposition features of the TGA transients.

FTIR spectra of GO and reduced GO pellets are shown in Figure 5. The peak observed at *ca.* 1720−1740 cm^{-1} can be assigned to the C═O (carbonyl) stretching. The C═C stretching peak from nonoxidized sp^2 C hydridization is centered on 1610 cm^{-1}. The peaks at 1400, 1220 and 1100 cm^{-1} correspond to C−OH, C−O−C, and C−O (alkoxy) vibrations, respectively. In comparison, the IR active features of the GO spectrum are clearly reduced in the reduced GO spectrum. The O−H stretching peak at

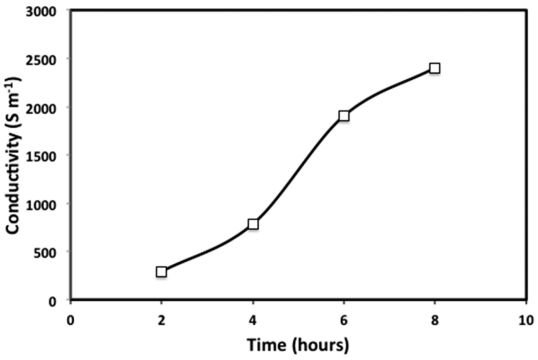

Figure 6. Plotted electrical conductivity values of the reduced GO, against reaction time, showing a clear increase in electrical conductivity as a function of time.

3400 cm^{-1} decreased significantly in terms of both intensity and fwhm and other peaks associated with oxygen containing functional groups are almost indistinguishable. This loss of characteristic oxygen spectral features indicates a significant degree of hydroxyl and carbonyl functionalities are removed on reduction of the GO material.

As a result of the oxygenated functional groups densely decorating the graphene surface, GO is considered an electrically insulating material and thus the electrical conductivity of the reduced graphene oxide can be considered a valuable tool to determine the degree of the reduction occurring. The absence of electrical charging during SEM indicates that the graphene sheets are electrically conductive and this qualitative conclusion was further confirmed by DC electrical measurements. Free-standing reduced graphene oxide papers were prepared *via* filtration of the colloidal suspension through an Anodisc membrane filter (47 mm in diameter, 0.2-μm pore size, Whatman, Middlesex, UK).[29] The free-standing papers were cut into strips for measurement. The conductivity of the reduced GO papers was found to increase proportionally with reaction time, and is associated with the increasing degree of functionality removal during reaction, as indicated in Figure 6. After 8 h reduction, electrical conductivity was measured to be *ca.* 2400 S m^{-1}. This value is similar to the conductivity measured for pristine graphite (2500 ± 15 S m^{-1}),[17] 50 times higher than the conductivity of GO reduced by $NaBH_4$ (46.7 S m^{-1}),[23] and only 10 times less than the highest value reported to date for a self-supporting graphene-based material (32 000 S m^{-1})

Scanning electron microscopy (SEM) of the reduced GO sample gleaned a very interesting surface morphology. While reduced GO prepared *via* wet-chemical and thermal reduction routes tends to aggregate, forming a disordered solid, the graphene sheets in the present work are loose and display minimal reaggregation. The heavily corrugated and highly convoluted rGO structure minimizes the face-to-face restacking of the sheets, leading to high surface area

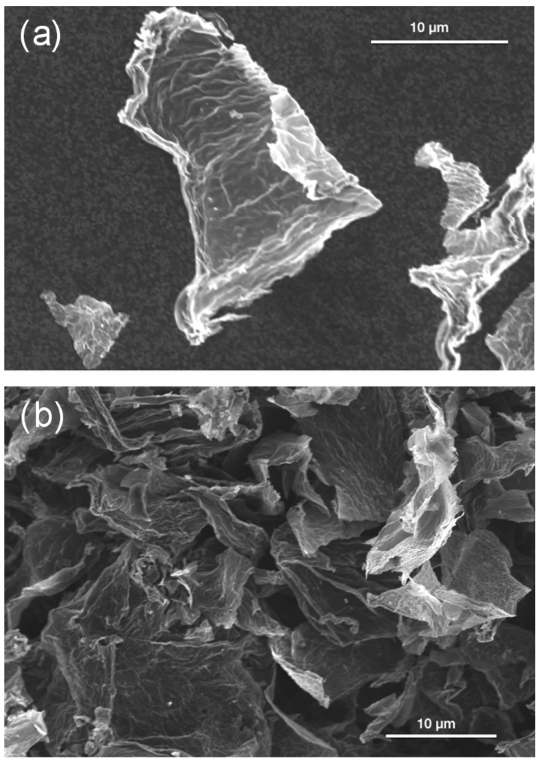

Figure 7. (a) SEM images showing both exhibiting flake "corrugation" or "ripples" as well as a lack of flake-aggregation, as can be seen in (b) where individual flakes can be identified.

materials and opening the door to potential supercapacitor applications. In order to achieve optimum electrical capacitance, it is crucial to maintain a high surface area during electrode manufacture, and for said purpose a suspension of reduced GO in NMP was prepared *via* sonication. The suspension was then dip-coated into a preheated (100 °C) current collector and dried at 250 °C under a vacuum. This process was repeated several times in order to completely cover the current collector with reduced GO material. It is noteworthy that the electrode fabrication was performed without the employment of a binder or conductive agent, such as carbon black, which is commonly employed in such studies. Interestingly the reduced graphene layers were stable despite the prior heating and quenching stages, and the manufactured electrode maintained the highly convoluted structure as presented in Figure 7.

Cyclic voltammetry and galvanostatic charge–discharge cycling data were obtained in 6 M KOH solution. The cyclic voltammograms (Figure 8) clearly show near-rectangular shape at different scan rates, typically associated with purely capacitive behavior, and indicates that the rGO formed *via* this route possesses a high specific electrochemical double-layer capacitance. It can be seen that the measured capacitance is also proportional to the scan rate of the recorded voltammograms.

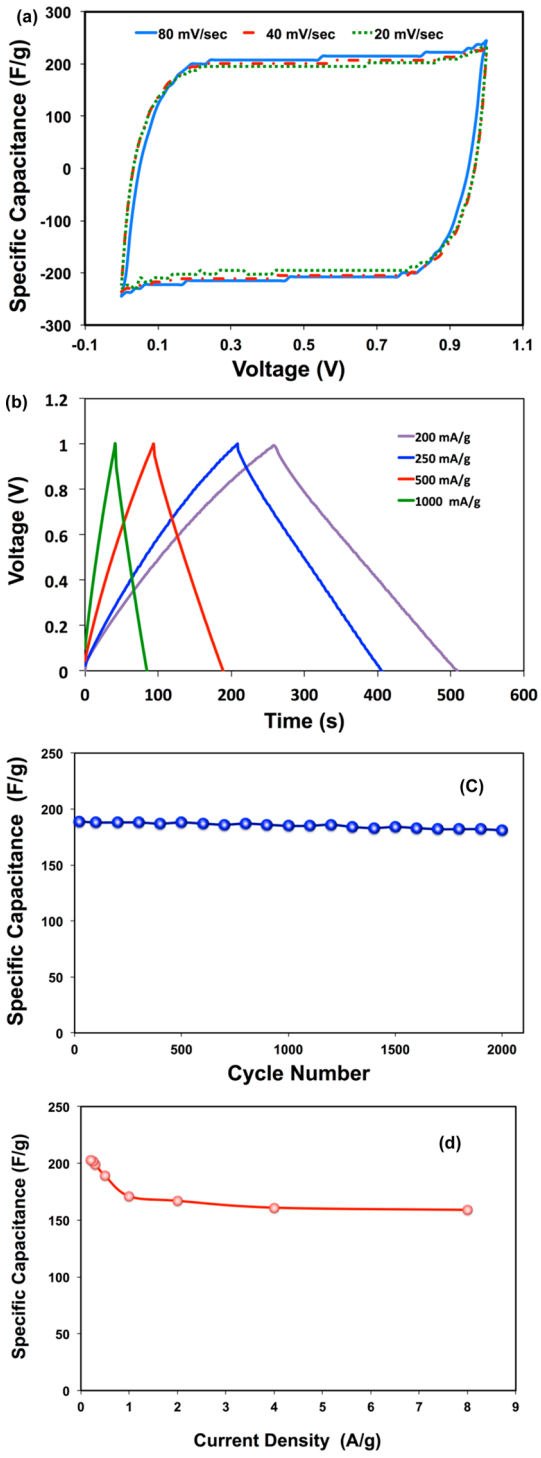

Figure 8. Supercapacitance performance of the reduced graphene oxide prepared using Li in molten LiCl–KCl at 370 °C, and measured in 6 M KOH electrolyte. (a) CV curves for different scan rates from 20 to 80 mV sec^{-1} showing rectangular shapes indicative of capacitive behavior. (b) Galvanostatic charge/discharge under different constant current values, showing fast charge transfer rates and the absence of an observable voltage drop. (c) Cycling stability of the supercapacitor at 0.5 A g^{-1} constant current cycling. Retention of 97% was obtained after 10 000 cycles. (d) Specific capacitance as a function of the current densities calculated from the corresponding discharge curve for each current density.

TABLE 1. Comparison of Measured Parameters of Reduced Graphene Oxide from Different Reduction Method

process	C/O ratio	electrical conductivity (S/m)	specific capacitance (F/g)	specific surface area (m^2/g)	specific capacitance retention %
Reduction by microwave irradiation then activated by KOH.[33]	35	500 (pressed powder)	200 ionic liquid	3100 (activated)	97 after 10000 cycles
Reduction by hydrazine at 100 °C.[8]	11.5	200 (pressed powder)	135 KOH	705	unknown
Reduction with Hydrazine vapor at low pressure.[34]	7.3	100 film	205 KOH	320	90 after 1200 cycles
Thermal reduction at 200 °C under a high vacuum (below 1 Pa).[35]	10	unknown	122 KOH	350	~94 after 100 cycles
Solvothermal reduction in propylene carbonate at 150 °C.[36]	8.3	2100 (paper-like)	120 organic	unknown	unknown
Reduction with hydrobromic acid at 110 °C.[37]	3.9	0.023	348 in H_2SO_4 and 158 in ionic liquid >(pseudocapacitance involved)	unknown	increased to 125 after 1800 cycle
Thermal reduction at 1050 °C.[38]	10[15]	2300 (pressed powder)[15]	117 H_2SO_4	925	unknown
Solvothermal reduction in DMF at 150 °C.[39]	5.97	unknown	276 H_2SO_4 (pseudocapacitance involved)	unknown	increased to 106 after 1980 cycles
Reduction with urea at 95 °C.[40]	4.5	43 (paper-like)	255 H_2SO_4 (pseudocapacitance involved)	590	93 after 1200 cycles
Reduction with urea at 95 °C followed by annealing at 800 °C under nitrogen.[40]	19.7	4520 (annealed paper)	172 H_2SO_4	630	94 after 1200 cycle
Hydrothermal reduction with sodium ascorbate at 95 °C.[41]	10.3	1 (hydrogel)	190 H_2SO_4[42] 186 solid state	414	93.6 after 10000 cycles
Reduction by laser irradiation.[43]		1738 (film)	204 solid state	1520	95 after 1000 cycles
Reduction by Li in molten LiCl–KCl at 370 °C (present work).	7	2400 (paper-like)	203 KOH	320	97 after 2000 cycles

The triangular shape of the charge–discharge transients at different current densities suggests high charge mobility at the electrodes. Figure 8 shows typical charge/discharge curves at different current densities. The absence of a voltage drop at the beginning of the discharge curve suggests a small internal resistance for the reduced graphene oxide electrode, which is further evidence of oxygen-containing functional group removal. The specific capacitance measured at a current density of 0.2 A g^{-1} was *ca.* 203 F g^{-1}. This is very similar to the values reported for graphene electrodes (205–215 F g^{-1}),[30,31] cross-linked reduced graphene oxide (211 F g^{-1}),[32] and much higher than that quoted for GO reduced by hydrazine monohydrate (135 F g^{-1}) (Table 1).

A Proposed Reduction Mechanism. Control experiments have been performed in order to probe the reduction mechanism, with respect to both lithium and the molten salt. Molten lithium at 225 °C was employed as the reducing agent on which the GO was supported. However, no apparent reduction was observed in the Raman or in the XRD trace (see Supporting Information). After termination of the experiment, a solid layer byproduct covering the lithium was visible, perhaps preventing further lithium reduction.

Reduction using Li vapor *via* suspension of the GO on an airtight argon field reactor (see Supporting Information) also yielded materials with C/O ratio of 3.8 and no significant observable changes were observed on the Raman trace. A solid layer byproduct was again visible, on the floor of the reaction vessel covering the remaining Li. Both of these procedures highlight the requirement for the molten salts' employment as a flux, or slag, in which simultaneous dissolution of the reduction side-products can proceed, allowing a continued and unhindered reduction of the GO materials. Reaction rates measured in the absence of Li containing molten salts were found to be very slow. After 24 h GO immersion in molten LiCl–KCl, the inherent oxygen content decreased slightly as can be seen from increasing the C/O ratio from 2.2 to 2.8.

It can be predicted from such results, that both the reaction rate and the reduction power of any alkali metal-molten salts system are dependent upon two factors: (1) the solubility of the reduction product (MOH in its simple form; where M is an alkali metal), and (2) the solubility of the reducing agent in the same molten salt. Therefore, another set of experiments has been conducted to confirm the effect of these two factors.

The solubility of Li and of oxide ions is much higher in molten LiCl than in the eutectic mixture. Therefore, one could expect more reduction from Li in molten LiCl. The C/O ratio of the GO reduced with Li in molten LiCl was measured to be 10.4 after 4 h of the reduction; about twice the value measured when the eutectic mixture was used. A further improvement in deoxygenating GO was observed when Ca was used as a

reducing agent in molten $CaCl_2$. The C/O ratio increased to 14.5 after only 2 h of reduction. The Raman analysis results also confirmed this improvement. While the I_D/I_G ratio was found to be 0.22 when Li was used in the eutectic mixture after 8 h, it took only 4 h to achieve this value in molten LiCl, and 2 h with Ca in molten $CaCl_2$. Considering the increase of the solubility of the reducing agent and the oxide ions in the order LiCl−KCl → LiCl→ $CaCl_2$,[44] it is clear that the mechanism of the reduction is through reaction 1 with the molten salts working as a flux to host the reducing agent and dissolve the reaction products and consequently improve the reaction kinetics.

$$GO-H + Li \Rightarrow rGO + LiOH \quad (1)$$

CONCLUSIONS

We present a method for the successful reduction of GO materials using alkali metal in molten halide, employing the use of several characterization tools to probe the degree of functionality of the resulting materials. XPS and FTIR spectroscopy show a significantly reduced degree of oxygen containing functionalities, and Raman spectroscopy shows that the rGO materials' chemical structure resembles nonoxygenated materials. XRD shows that interplanar gallery contraction occurs during reduction, and is explained by the removal of oxygenated species located between neighboring graphene sheets allowing conjugated sp^2 network recovery.

Finally, the reduced GO materials show good conductivity (2400 S m^{-1} *cf.* 2500 S m^{-1} observed for pristine graphite materials), and SEM imaging shows materials exhibiting surface corrugation, an ideal morphology when considering employment in supercapacitors, where it is essential to maintain high surface area systems with a minimum tendency to restacking. To strengthen this, electrochemical capacitance measurements yielded an impressive specific capacitance of 203 F g^{-1}, *cf.* 205−215 F g^{-1} for graphene-based electrochemical capacitors, and galvanostatic cycling presents fast charge mobility at the electrode/electrolyte interface.

EXPERIMENTAL SECTION

Preparation and Reduction of Graphene Oxide. Graphene oxide was prepared by a modified Hummers' method. Lithium chloride (LiCl, Aldrich, 99.99%), and potassium chloride (KCl, Aldrich, 99.99%) were dried separately at 200°C under a vacuum for 48 h. The salts were mixed at their eutectic compositions and kept under a dry atmosphere in a glovebox. About 0.7 g of lithium powder and 0.2 g of GO were then added to 120 g of the salt, and the mixture charged into an alumina crucible. The alumina crucible was then taken from the glovebox and placed at the bottom of an airtight alumina vessel that served as the molten salt reactor. The alumina vessel was sealed from the top using solid silicone stopper that has 2 openings to allow argon gas circulation. The alumina vessel (70 mm internal diameter, 700 mm height) was then placed in a programmable vertical furnace where the temperature was maintained at 120 °C to remove any residual moisture. The temperature was then increased to 370 °C and held for the required time. During that period, the samples were stirred manually every 10 min using a 3 mm diameter stainless steel rod attached to the silicone stopper seal. Samples were allowed to cool in the furnace under argon flow. After removal from the reactor, the solidified salt was immersed in 2 L of hot water to help dissolve the majority of the salt. The reduced GO powder was collected by centrifugation. The water washing and centrifugation steps were repeated twice to remove the salt residue. The sample was then washed with ethanol and dried overnight at 60 °C in a vacuum oven. The same procedure was used for the noneutectic reduction processes, with Li in molten LiCl, and Ca in molten $CaCl_2$ with holding temperatures of 700 and 900 °C respectively. More details on preparing anhydrous $CaCl_2$ can be obtained elsewhere.[45]

Characterization. XRD analysis was conducted using a Philips X'PERT APD powder X-ray diffractometer (λ = 1.54 Å, Cu Kα radiation). Raman spectra were obtained using a Renishaw 1000 spectrometer coupled to a 633 nm He−Ne laser. The laser spot size was ~1−2 μm, and the power was about 1 mW when the laser was focused on the sample using an Olympus BH-1 microscope. Fourier-transform IR (FTIR) spectroscopy was performed at room temperature using a Varian 3100 FTIR spectrometer. The samples were ground with potassium bromide and then pressed into disks. Scanning electron microscopy (SEM) was performed using a Philips XL30 FEG SEM, operating at an accelerating voltage of 5 kV. Thermogravimetric analysis (TGA) was performed using Jupiter Netzsch STA 449 C instrument heated at 10 degrees per minute from room temperature to 700 °C under nitrogen gas flow. X-ray photoelectron spectroscopy (XPS) were collected using a Kratos Axis Ultra X-ray photoelectron spectrometer, equipped with an aluminum/magnesium dual anode and a monochromated aluminum X-ray sources.

Preparation of Electrodes and Electrochemical Characterization. Reduced GO paste was formed by adding about 10 mL of *N*-methylpyrrolidone (NMP) and sonicating for 20 min. The paste was then dip-coated onto nickel foam and dried under a vacuum at 250 °C for 24 h. This step was repeated twice to deposit more layers onto the 1.5 cm diameter nickel foam current collector. The weight of the active materials was ~6 mg. The capacitance was measured in the two-electrode configuration, with a Whatman filter paper as a separator, and 6 M aqueous KOH as the electrolyte. Cyclic voltammetry (CV) and galvanostatic charge/discharge were carried out using an Iviumstat Electrochemical Interface. The recommended practical method to calculate the capacitance was used, as described elsewhere.[46]

Conflict of Interest: The authors declare no competing financial interest.

Acknowledgment. The authors acknowledge financial support from the U.K. EPSRC (grant references EP/I023879/1 and EP/K016954/1) and the University of Manchester EPS strategic fund.

Supporting Information Available: Details of the control experiments methods and setup, details on the method used to calculate the specific capacitance, comparison of the times required for GO reduction by different methods, carbon to oxygen ratio for the GO reduced without molten salt flux, the capacitance of the Ni Foam current collector, wide scan XPS for the reduced GO in Li-LiCl−KCl molten salts at 370 °C. This material is available free of charge *via* the Internet at http://pubs.acs.org.

REFERENCES AND NOTES

1. Geim, A. K. Graphene: Status and Prospects. *Science* **2009**, *324*, 1530–1534.

2. Balandin, A.; Ghosh, S.; Bao, W. Superior Thermal Conductivity of Single-Layer Graphene. *Nano Lett.* **2008**, *8*, 902–907.
3. Lee, C.; Hone, J. Measurement of the Elastic Properties and Intrinsic Strength of Monolayer Graphene. *Science* **2008**, *321*, 385–388.
4. Geim, A. K.; MacDonald, A. H. Graphene: Exploring Carbon Flatland. *Phys. Today* **2007**, *60*, 35–41.
5. Geim, A. K.; Novoselov, K. S. The Rise of Graphene. *Nat. Mater.* **2007**, *6*, 183–191.
6. Blake, P.; Brimicombe, P. D.; Nair, R. R.; Booth, T. J.; Jiang, D.; Schedin, F.; Ponomarenko, L. A.; Morozov, S. V.; Gleeson, H. F.; Hill, E. W.; Geim, A. K.; Novoselov, K. S. Graphene-Based Liquid Crystal Device. *Nano Lett.* **2008**, *8*, 1704–1708.
7. Schedin, F.; Geim, A. K.; Morozov, S. V.; Hill, E. W.; Blake, P.; Katsnelson, M. I.; Novoselov, K. S. Detection of Individual Gas Molecules Adsorbed on Graphene. *Nat. Mater.* **2007**, *6*, 652–655.
8. Stoller, M. D.; Park, S.; Yanwu, Z.; An, J.; Ruoff, R. S. Graphene-Based Ultracapacitors. *Nano Lett.* **2008**, *8*, 3498–3502.
9. Stankovich, S.; Dikin, D. A.; Dommett, G. H. B.; Kohlhaas, K. M.; Zimney, E. J.; Stach, E. A.; Piner, R. D.; Nguyen, S. T.; Ruoff, R. S. Graphene-Based Composite Materials. *Nature* **2006**, *442*, 282–286.
10. Hernandez, Y.; Nicolosi, V.; Lotya, M.; Blighe, F. M.; Sun, Z.; De, S.; McGovern, I. T.; Holland, B.; Byrne, M.; Gun'ko, Y. K.; Boland, J. J.; Niraj, P.; Duesberg, G.; Krishnamurthy, S.; Goodhue, R.; Hutchison, J.; Scardaci, V.; Ferrari, A. C.; Coleman, J. N. High-Yield Production of Graphene by Liquid-Phase Exfoliation of Graphite. *Nat. Nanotechnol.* **2008**, *3*, 563–568.
11. Abdelkader, A. M.; Kinloch, I. A.; Dryfe, R. A. W. Continuous Electrochemical Exfoliation of Micrometer-Sized Graphene Using Synergistic ion Intercalations and Organic Solvents. *ACS Appl. Mater. Interfaces* **2014**, *6*, 1632–1639.
12. Cooper, A. J.; Wilson, N. R.; Kinloch, I. A.; Dryfe, R. A. W. Single Stage Electrochemical Exfoliation Method for the Production of Few-Layer Graphene *via* Intercalation of Tetraalkylammonium Cations. *Carbon* **2014**, *66*, 340–350.
13. Cooper, A. J.; Velický, M.; Kinloch, I. A.; Dryfe, R. A. W. on the Controlled Electrochemical Preparation of R4N+ Graphite Intercalation Compounds and Their Host Structural Deformation Effects. *J. Electroanal. Chem.* **2014**, *730*, 34–40.
14. Abdelkader, A. M.; Kinloch, I. A.; Dryfe, R. A. W. High-Yield Electro-oxidative Preparation of Graphene Oxide. *Chem. Commun.* **2014**, *50*, 8402–8404.
15. Schniepp, H. C.; Li, J.-L.; McAllister, M. J.; Sai, H.; Herrera-Alonso, M.; Adamson, D. H.; Prud'homme, R. K.; Car, R.; Saville, D. A.; Aksay, I. A. Functionalized Single Graphene Sheets Derived from Splitting Graphite Oxide. *J. Phys. Chem. B* **2006**, *110*, 8535–8539.
16. Wang, X.; Zhi, L.; Mullen, K. Transparent, Conductive Graphene Electrodes for Dye-Sensitized Solar Cells. *Nano Lett.* **2007**, *8*, 323–327.
17. Stankovich, S.; Dikin, D. A.; Piner, R. D.; Kohlhaas, K. A.; Kleinhammes, A.; Jia, Y.; Wu, Y.; Nguyen, S. T.; Ruoff, R. S. Synthesis of Graphene-Based Nanosheets *via* Chemical Reduction of Exfoliated Graphite Oxide. *Carbon* **2007**, *45*, 1558–1565.
18. Si, Y.; Samulski, E. T. Synthesis of Water Soluble Graphene. *Nano Lett.* **2008**, *8*, 1679–1682.
19. Hofmann, U.; Frenzel, A. Die Reduktion von Graphitoxyd mit Schwefelwasserstoff. *Kolloid-Z.* **1934**, *68*, 149–151.
20. Zhao, J.; Pei, S.; Ren, W.; Gao, L.; Cheng, H.-M. Efficient Preparation of Large-Area Graphene Oxide Sheets for Transparent Conductive Films. *ACS Nano* **2010**, *4*, 5245–5252.
21. Moon, I. K.; Lee, J.; Ruoff, R. S.; Lee, H. Reduced Graphene Oxide by Chemical Graphitization. *Nat. Commun.* **2010**, *1*, 73.
22. Wang, G.; Yang, J.; Park, J.; Gou, X.; Wang, B.; Liu, H.; Yao, J. Facile Synthesis and Characterization of Graphene Nanosheets. *J. Phys. Chem. C* **2008**, *112*, 8192–8195.
23. Gao, W.; Alemany, L. B.; Ci, L.; Ajayan, P. M. New Insights into the Structure and Reduction of Graphite Oxide. *Nat. Chem.* **2009**, *1*, 403–408.
24. Fan, Z.-J.; Kai, W.; Yan, J.; Wei, T.; Zhi, L.-J.; Feng, J.; Ren, Y.-m.; Song, L.-P.; Wei, F. Facile Synthesis of Graphene Nanosheets *via* Fe Reduction of Exfoliated Graphite Oxide. *ACS Nano* **2010**, *5*, 191–198.
25. Mei, X.; Ouyang, J. Ultrasonication-Assisted Ultrafast Reduction of Graphene Oxide by Zinc Powder at Room Temperature. *Carbon* **2011**, *49*, 5389–5397.
26. Fan, Z.; Wang, K.; Wei, T.; Yan, J.; Song, L.; Shao, B. An Environmentally Friendly and Efficient Route for the Reduction of Graphene Oxide by Aluminum Powder. *Carbon* **2010**, *48*, 1686–1689.
27. Kaniyoor, A.; Ramaprabhu, S. A Raman Spectroscopic Investigation of Graphite Oxide Derived Graphene. *AIP Adv.* **2012**, *2*, 032183-13.
28. Zhang, K.; Zhang, L. L.; Zhao, X. S.; Wu, J. Graphene/Polyaniline Nanofiber Composites as Supercapacitor Electrodes. *Chem. Mater.* **2010**, *22*, 1392–1401.
29. Park, S.; An, J.; Jung, I.; Piner, R. D.; An, S. J.; Li, X.; Velamakanni, A.; Ruoff, R. S. Colloidal Suspensions of Highly Reduced Graphene Oxide in a Wide Variety of Organic Solvents. *Nano Lett.* **2009**, *9*, 1593–1597.
30. Wang, Y.; Shi, Z.; Huang, Y.; Ma, Y.; Wang, C.; Chen, M.; Chen, Y. Supercapacitor Devices Based on Graphene Materials. *J. Phys. Chem. C* **2009**, *113*, 13103–13107.
31. Yang, X.; Zhu, J.; Qiu, L.; Li, D. Bioinspired Effective Prevention of Restacking in Multilayered Graphene Films: Towards the Next Generation of High-Performance Supercapacitors. *Adv. Mater.* **2011**, *23*, 2833–2838.
32. Tang, L. A. L.; Lee, W. C.; Shi, H.; Wong, E. Y. L.; Sadovoy, A.; Gorelik, S.; Hobley, J.; Lim, C. T.; Loh, K. P. Highly Wrinkled Cross-Linked Graphene Oxide Membranes for Biological and Charge-Storage Applications. *Small* **2012**, *8*, 423–431.
33. Zhu, Y.; Murali, S.; Stoller, M. D.; Ganesh, K. J.; Cai, W.; Ferreira, P. J.; Pirkle, A.; Wallace, R. M.; Cychosz, K. A.; Thommes, M.; Su, D.; Stach, E. A.; Ruoff, R. S. Carbon-Based Supercapacitors Produced by Activation of Graphene. *Science* **2011**, *332*, 1537–1541.
34. Wang, Y.; Shi, Z. Q.; Huang, Y.; Ma, Y. F.; Wang, C. Y.; Chen, M. M.; Chen, Y. S. Supercapacitor Devices Based on Graphene Materials. *J. Phys. Chem. C* **2009**, *113*, 13103–13107.
35. Lv, W.; Tang, D. M.; He, Y. B.; You, C. H.; Shi, Z. Q.; Chen, X. C.; Chen, C. M.; Hou, P. X.; Liu, C.; Yang, Q. H. Low-Temperature Exfoliated Graphenes: Vacuum-Promoted Exfoliation and Electrochemical Energy Storage. *ACS Nano* **2009**, *3*, 3730–3736.
36. Zhu, Y. W.; Stoller, M. D.; Cai, W. W.; Velamakanni, A.; Piner, R. D.; Chen, D.; Ruoff, R. S. Exfoliation of Graphite Oxide in Propylene Carbonate and Thermal Reduction of the Resulting Graphene Oxide Platelets. *ACS Nano* **2010**, *4*, 1227–1233.
37. Chen, Y.; Zhang, X.; Zhang, D.; Yu, P.; Ma, Y. High Performance Supercapacitors Based on Reduced Graphene Oxide in Aqueous and Ionic Liquid Electrolytes. *Carbon* **2011**, *49*, 573–580.
38. Vivekchand, S. R. C.; Rout, C. S.; Subrahmanyam, K. S.; Govindaraj, A.; Rao, C. N. R. Graphene-Based Electrochemical Supercapacitors. *J. Chem. Sci.* **2008**, *120*, 9–13.
39. Lin, Z.; Liu, Y.; Yao, Y.; Hildreth, O. J.; Li, Z.; Moon, K.; Wong, C.-p. Superior Capacitance of Functionalized Graphene. *J. Phys. Chem. C* **2011**, *115*, 7120–7125.
40. Lei, Z.; Lu, L.; Zhao, X. S. The Electrocapacitive Properties of Graphene Oxide Reduced by Urea. *Energy Environ. Sci.* **2012**, *5*, 6391–6399.
41. Sheng, K.-x.; Xu, Y.-x.; Li, C.; Shi, G.-q. High-Performance Self-Assembled Graphene Hydrogels Prepared by Chemical Reduction of Graphene Oxide. *New Carbon Mater.* **2011**, *26*, 9–15.
42. Xu, Y.; Lin, Z.; Huang, X.; Liu, Y.; Huang, Y.; Duan, X. Flexible Solid-State Supercapacitors Based on Three-Dimensional Graphene Hydrogel Films. *ACS Nano* **2013**, *7*, 4042–4049.
43. El-Kady, M. F.; Strong, V.; Dubin, S.; Kaner, R. B. Laser Scribing of High-Performance and Flexible Graphene-Based Electrochemical Capacitors. *Science* **2012**, *335*, 1326–1330.

44. Abdelkader, A. M.; Kilby, K. T.; Cox, A.; Fray, D. J. DC Voltammetry of Electro-deoxidation of Solid Oxides. *Chem. Rev.* **2013**, *113*, 2863–2886.
45. Abdelkader, A. M.; Fray, D. J. Direct Electrochemical Preparation of Nb-10Hf-1Ti Alloy. *Electrochim. Acta* **2010**, *55*, 2924–2931.
46. Stoller, M. D.; Ruoff, R. S. Best Practice Methods for Determining an Electrode Material's Performance for Ultracapacitors. *Energy Environ. Sci.* **2010**, *3*, 1294–1301.